Available online at www.sciencedirect.com

SciVerse ScienceDirect

Ceramics International 39 (2013) 7107–7113

CERAMICS INTERNATIONAL

www.elsevier.com/locate/ceramint

Cu-doped TiO_2 nanoparticles/graphene composites for efficient visible-light photocatalysis

N.R. Khalid[a,b,*], E. Ahmed[a], Zhanglian Hong[b,**], M. Ahmad[a,b], Yuewei Zhang[b], Sadia Khalid[a]

[a]Department of Physics, Bahauddin Zakariya University, Multan 60800, Pakistan

[b]State Key Laboratory of Silicon Materials and Department of Materials Science and Engineering, Zhejiang University, Hangzhou 310027, PR China

Received 3 February 2013; received in revised form 5 February 2013; accepted 17 February 2013
Available online 26 February 2013

Abstract

Cu-doped TiO_2/graphene (Cu–TiO_2/GR) composites were successfully synthesized by a simple hydrothermal method. The coating of anatase TiO_2 nanoparticles on the whole graphene was confirmed by X-ray diffraction (XRD), transmission electron microscopy (TEM), and X-ray photoelectron spectroscopy (XPS). UV–visible diffuse reflectance spectroscopy (DRS) showed that the resulting Cu–TiO_2/GR composites exhibited extended light absorption in visible-light region compared with pure TiO_2. Photoluminescence emission spectra of Cu–TiO_2/GR composites showed better charge separation capability as compared to Cu/TiO_2 and pure TiO_2. The photocatalytic activity was evaluated by degradation of methyl orange (MO) dye under visible-light irradiation. The results demonstrate that Cu–TiO_2/GR composite can effectively photodegrade MO, and show an excellent photocatalytic enhancement over pure TiO_2. It was concluded that the synergistic effects of the great adsorptivity of dyes, extended light absorption range and efficient charge separation played a significant role for the enhancement of photoactivity of Cu–TiO_2/GR composite catalyst.

Keywords: A. Sol–gel processes; B. Nanocomposites; C. Optical properties; D. TiO_2

1. Introduction

Titanium dioxide (TiO_2) is the most widely used semiconductor in environmental pollution control, conversion and energy storage, sensors, photovoltaics and Li batteries because of its unique photo-electric properties, high chemical stability, low cost and safety toward both humans and the environment [1–4]. The improvement and optimization of TiO_2 as photocatalyst is a major task for technical applications of heterogeneous photocatalysis in the future. In this sense, many investigations for the enhancement of photocatalytic activity either in UV or visible region have been carried out [5–9]. However, many problems remain unresolved for practical applications, such as narrow light response range and low separation probability of the photoinduced electron–hole pairs in TiO_2 photocatalytic system. In order to improve the photocatalytic activity as well as the response into visible-light region, TiO_2 doping with transition metals has been widely investigated [10–15]. However, the metal selective doping is one of the common approaches to enhance the phtocatalytic efficiency of the catalyst. Cu^{2+} with redox potentials of 0.16 V (Cu^{2+}/Cu^{+}) and 0.52 V (Cu^{2+}/Cu) versus the normal hydrogen electrode has been found to be a good modifier for various visible-light responsive photocatalysts [12–15]. The electron generated from the excitation of photocatalyst is directly trapped by Cu^{2+}, which frees up the oxidative valence hole of the photocatalyst for the degradation of organic compounds. Therefore, metal ions doping can provide as charge trapping sites and thus reduce electron–hole recombination rate during photocatalysis.

In another method, it has been found that loading of TiO_2 nanoparticles on a co-adsorbent surface such as

*Corresponding author at: Department of Physics, Bahauddin Zakariya University, Multan 60800, Pakistan. Tel.: +92 61 9210091; fax: +92 61 9210098.

**Corresponding author. Tel./fax: +86 571 87951234.

E-mail addresses: khalidbzu@gmail.com (N.R. Khalid), hong_zhanglian@zju.edu.cn (Z. Hong).

0272-8842/$ - see front matter © 2013 Elsevier Ltd and Techna Group S.r.l. All rights reserved.
http://dx.doi.org/10.1016/j.ceramint.2013.02.051

mesoporous materials, zeolites, alumina, silica or carbon based materials is able to enhance the visible light photocatalytic activity of TiO_2 [16–19]. Among these, carbonaceous materials are of tremendous interest due to their unique pore structure, electronic properties and adsorption capacity. These materials include activated carbon, carbon nanotubes, and graphene [20–24]. Recently, graphene with its unique structure of one-atom thick planar sheets of sp^2-bonded carbon atoms closely packed in a honeycomb crystal lattice has attracted a great deal of scientific interest due to its excellent mechanical, electrical, thermal, and optical properties [24]. As compared with other carbonaceous materials, graphene has many advantages including high surface area and good interfacial contact with adsorbents. Therefore, it is desirable to explore simple and effective approaches for preparing graphene based composites and expand their practical applications. Graphene has a conjugated structure and the combination of TiO_2 and graphene may be an ideal preference to achieve an enhanced charge separation in electron-transfer processes. To the best of our knowledge, few investigations have been done on this topic. In a recent work, P25-TiO_2 dispersed on graphene nanosheet was reported to show enhanced photocatalytic activity [25]. Williams et al. mixed ultrasonically TiO_2 particles and graphene oxide (GO) colloids, followed by UV-assisted photocatalytic reduction of GO to yield TiO_2–graphene composites [26]. In another example, TiO_2–graphene composite materials were prepared by self-assembly of TiO_2 nanoparticles grown on graphene by a one-step approach with the assistance of an anionic surfactant [27]. Zhang et al. [23] demonstrated a facile and reproducible route (hydrothermal method) to obtain a P25–graphene composite for methyl blue degradation. Sonophototcatalytic activity of graphene oxide based Pt–TiO_2 composites for DBS degradation was studied by Neppolian et al. [28]. N. Farhangi et al. [29] prepared Fe doped TiO_2 nanowires on graphene sheets using supercritical CO_2 for photodegradation of 17β-estradiol (E_2).Thus, it will be advantageous to use the cooperative effect of metal ion doping like copper and coating TiO_2 nanoparticles on the surface of graphene sheets for enhancement of visible-light absorption response and photocatalytic activity.

In this study, Cu doped TiO_2 nanoparticles modified by graphene were prepared by a hydrothermal method. The effect of copper doping and graphene modification was investigated by degradation of methyl orange under visible-light irradiation. The Cu–TiO_2/GR composites showed higher photocatalytic activity and extended optical absorption in visible-light region.

2. Experimental section

2.1. Preparation of Cu doped TiO_2

Copper doped TiO_2 samples were synthesized by sol–gel method according to the report [30]. Firstly, the required amounts of tetrabutyl titanate and acetic acid (10 ml) were added to 50 ml absolute ethanol (solution A) in a beaker. Secondly, calculated amounts of $Cu(NO_3)_2 \cdot 3H_2O$, 5 ml acetic acid and 6.25 ml distilled water were added to 25 ml ethanol (solution B). In the next step, the solution B was added dropwise into solution A with vigorous magnetic agitation. The obtained mixture was stirred for 3 h, and then kept at 25 °C in air for 24 h to form aged homogeneous gel. The prepared gel was dried at 80 °C in a vacuum furnace. Moreover, the gel was porphyrized into powder and calcined at 450 °C in the furnace for 2 h to get Cu doped TiO_2 nanopowder. Finally, the atomic ratio of Cu doping into TiO_2 was varied from 0.5 to 2.0 at% and the samples obtained were labeled as 0.5Cu–TiO_2, 1.0Cu–TiO_2, and 2.0Cu–TiO_2.

2.2. Preparation of Cu–TiO_2/GR composites

Graphene oxide was synthesized from graphite powder (99.99% Alfa Aesar) by the Hummers method and details are given in our previous report [31,32]. Cu–TiO_2/GR composites were obtained via a hydrothermal method based on Zhang's work [23]. Briefly, 20 mg of graphene oxide was dissolved in a solution of 80 mL distilled (H_2O) and 40 mL ethanol by ultrasonic treatment for 2 h. Then 200 mg of TiO_2 or Cu–TiO_2 was added to the obtained graphene oxide solution and it was stirred for further 2 h to get a homogeneous suspension. In addition, the suspension was placed in a 200 mL Teflon-sealed autoclave at 120 °C for 3 h to simultaneously achieve the reduction of graphene oxide and deposition of TiO_2 on the graphene sheets. Finally, the resulting composite was recovered by filtration, rinsed with deionized water 10 times, and dried at 70 °C for 12 h in the vacuum furnace.

2.3. Sample characterization

The crystal structure of samples was characterized by powder X-ray diffraction (XRD) and patterns were collected from 10° to 80° in 2θ with 0.02° step/s using a Rigaku D/max-3B X-ray diffractometer with Cu Kα as radiation source ($\lambda = 0.15406$ nm) at 40 kV and 36 mA. Transmission electron spectroscopy (TEM) study was carried out on a JEOL JEM-1200EX electron microscope instrument operated at 200 kV. The samples for TEM were prepared by dispersing the final powder in ethanol; one drop of solution was then dropped on carbon–copper grids. Chemical compositions of the composites were analyzed using X-ray photoelectron spectroscopy (Thermo-VG Scientific, ESCALAB250, a monochromatic Al Kα X-ray source). The binding energy of the XPS spectra was calibrated with the reference to the C1s peak (284.6 eV) arising from adventitious carbon. UV–vis diffuse reflectance spectra (DRS) were recorded in the range of 300–800 nm using a HITACHI U-4100 UV–vis spectrometer with an integrating sphere accessory. The powders were pressed to form pellets, and $BaSO_4$ was used as a reference standard for correction of instrumental background. Their reflectance was

converted to absorbance by the Kubelka–Munk function: $F(R) \propto K/S = (1-R)^2/2R$, where K is the absorption coefficient, S is the scattering coefficient, and R is the diffuse reflectance. The PL emission spectra were recorded using an F-4500 Fluorescence Spectrophotometer (Hitachi). The samples were excited at 380 nm and the emission spectra were scanned between 400 and 700 nm wavelength ranges.

2.4. Measurement of photocatalytic activity

The photocatalytic activity of different samples was evaluated by monitoring the decomposition of methyl orange (MO) in a self-assembled apparatus with a metal halogen lamp (HQIBT, 400 W/D, OSRAM, Germany) as the radiation source. The visible-light ($\lambda \geq 420$ nm) used in the present investigation was obtained by a filter with cut-off wavelength of 420 nm. Typically, for the photocatalytic experiment, 100 mg catalyst was suspended in 100 mL MO aqueous solution with a concentration of 10 mg L^{-1} in a beaker. The suspension was magnetically stirred for 1 h to reach the adsorption/desorption equilibration before visible light exposure. Following this, the photocatalytic reaction was started by the exposure of visible light and the temperature of the suspension was kept at about 20 °C by an external cooling jacket with recycled water. After a setup exposure time, 5 ml suspension was sampled, centrifuged, and the supernatant liquid was taken out for UV–vis absorption spectrum. The intensity of the main absorption peak (464 nm) of the methyl orange dye was referred to as a measure of the residual MO dye concentration (C).

3. Results and discussion

XRD patterns of Cu doped TiO_2 and Cu–TiO_2/GR composites are shown in Fig. 1. The patterns clearly show peaks of TiO_2, namely, the planes (101), (004), (200), (211), (204), (220), and (215) at 2θ values of ca. 25.38°, 37.82°, 48.18°, 54.4°, 62.92°, 69.92°, and 74.9° respectively. All patterns were assigned to the polycrystalline anatase phase structure of TiO_2 according to (JCPDS-21-1272). In all Cu doped samples, no significant characteristics peaks of copper oxide were detected. It might be attributed to the lower copper content in these samples. The crystallite size of the samples was calculated from full-width at half-maxima of the (101) peak of anatase TiO_2 by the Debye–Sherrer equation:

$$d = k\lambda / \beta \cos\theta$$

where d represents the crystallite size of, λ represents the wavelength of incident X-ray, β is full width at half maximum (FWHM) of diffraction peak and θ represents the scattering angle. The average crystallite size calculated from above equation for pure TiO_2 was 9.5 nm and for 0.5Cu–TiO_2, 1.0Cu–TiO_2, and 2.0 Cu–TiO_2 samples was 8.8 nm, 7.7 nm and 6.9 nm respectively. These results show that Cu doping can inhibit the growth of TiO_2 crystallites [33]. Furthermore, absence of graphene peaks in the XRD patterns of composite catalysts shows that graphene did not change the structure of TiO_2 [34].

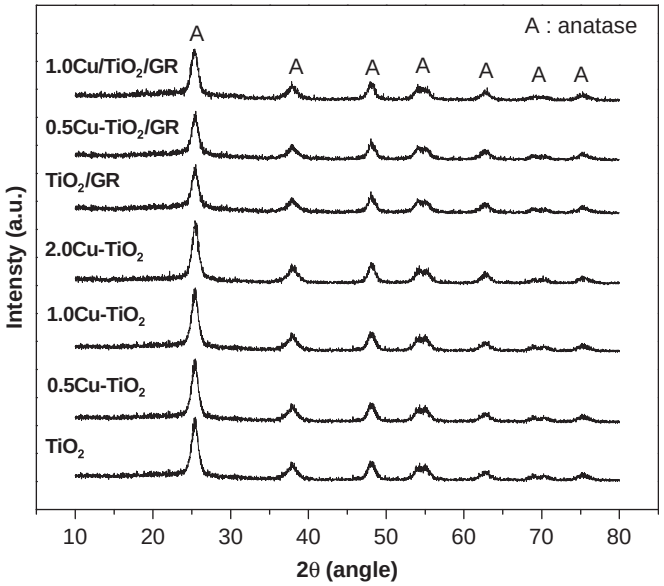

Fig. 1. XRD patterns of Cu–TiO_2 and Cu–TiO_2/GR composites samples with various copper contents.

TEM images of TiO_2 and 1.0Cu–TiO_2 nanoparticles are shown in Fig. 2a and b, respectively. In these images, the primary particles are quite uniform in nearly spherical morphology and their size (9–12) is consistent with those calculated from XRD measurement. Fig. 2c and d shows the image results of TiO_2/GR and 1.0Cu–TiO_2/GR composites, respectively which show that TiO_2 and Cu–TiO_2 nanoparticles were successfully deposited and randomly distributed on graphene sheets after the hydrothermal process.

Fig. 3 shows the XPS survey spectra of 1.0Cu–TiO_2/GR composite. The composite contains 0.7% Cu2p, 49.3% O1s, 24% Ti2p and 26% C1s. Fig. 4a shows a high resolution spectrum of Ti2p; the Ti2p3/2 and Ti2p1/2 are located at binding energies of 459.4 eV and 465.0 eV respectively, which agree with the values of Ti^{4+} in the TiO_2 lattice [35]. Fig. 4b shows the highly resolved O1s core level spectrum having main peak at 530.0 eV, which could be attributed to the metallic oxides Ti–O bond, in agreement with binding energy of O^{2-} in the TiO_2 lattice and the peak appearing at 532.0 eV was ascribed to the adsorbed OH^- on the surface of TiO_2 [36]. In core level XPS spectrum of C1s as shown in Fig. 4c, the main peak was observed at 284.5 eV, which corresponds to the adventitious carbon adsorbed on the surface of sample [37]. The peak at 286.7 eV suggests the existence of C–O bonds of carbonate species and the peak at 289.25 eV corresponds to C=C bonds [29,36]. In Fig. 4d the two peaks of Cu2p at 933 eV and 953.4 corresponds to Cu2p3/2 and Cu2p1/2, respectively. These results show that loaded copper existed as Cu^{2+} in the Cu–TiO_2/GR composite [6,33].

UV–vis diffuse reflectance spectra of Cu–TiO_2 and Cu–TiO_2/GR composite catalysts as well as of pure TiO_2 are

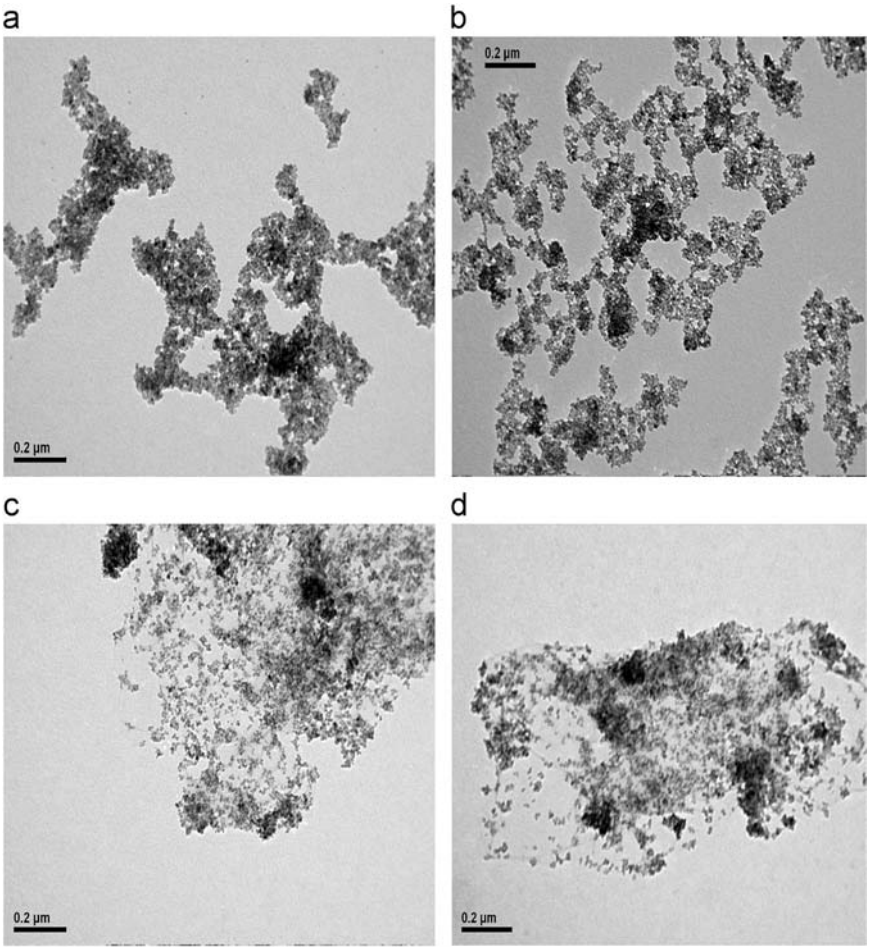

Fig. 2. TEM images of (a) TiO_2, (b) 1.0Cu–TiO_2, (c) TiO_2/GR, and (d) 1.0Cu–TiO_2/GR.

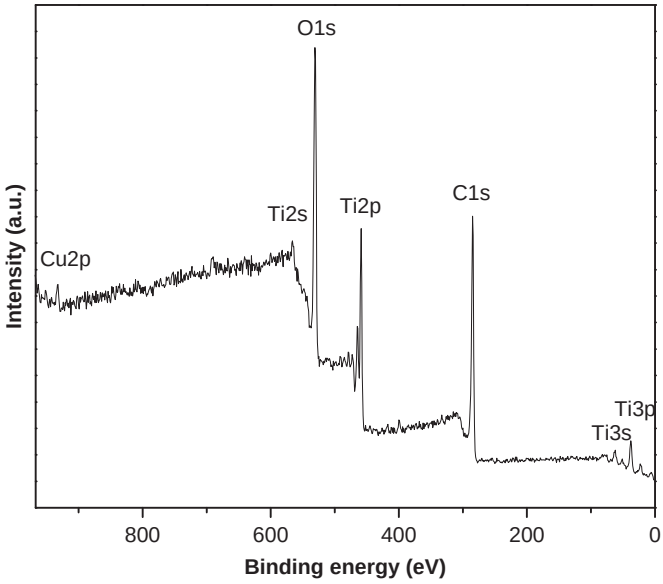

Fig. 3. XPS survey spectra of 1.0Cu–TiO_2/GR composite catalyst.

shown in Fig. 5. The spectrum of pure TiO_2 shows the absorption edge to be about 388 nm, as commonly observed for anatase TiO_2, while copper doping greatly enhanced the absorption in visible-light region with increasing copper content. The absorption band between 400 and 500 nm might be assigned to presence of Cu^{1+} clusters in partially reduced CuO matrix as well as $(Cu–O–Cu)^{+}$ clusters. A band between 600 and 800 nm indicates crystalline and bulk CuO

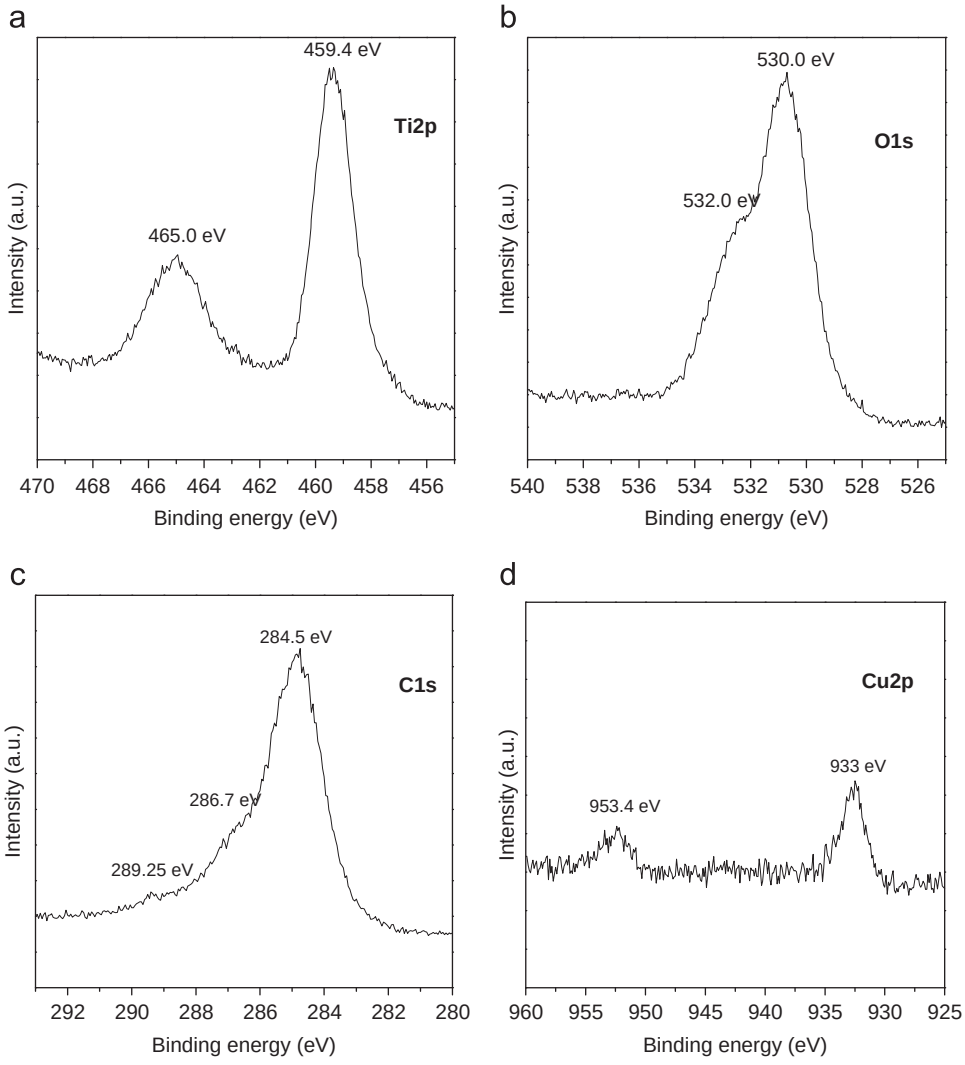

Fig. 4. High resolution XPS spectra of (a) Ti2p region, (b) O1s region, (c) C 1s region and (d) Cu 2p region for 1.0Cu–TiO_2/GR composite.

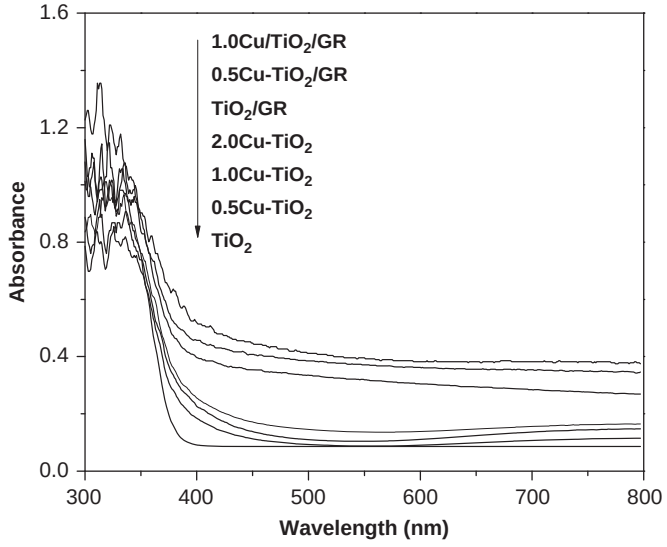

Fig. 5. UV–vis DRS of TiO_2, Cu–TiO_2 and Cu–TiO_2/GR composites photocatalysts.

in octahedral symmetry [6,11]. Furthermore, a noticable increased absorption in visible-light region was observed after modification of Cu doped TiO_2 nanoparticles with graphene, which might be attributed to the fact that incorporation of graphene increased absorption of TiO_2 in visible-light range, similar to TiO_2–CNT and C-doped TiO_2 [23]. Thus, it can be inferred that doping with a transition metal ion such as copper and incorporation of graphene are effective for visible-light response and will play a significant role for enhancing the photocatalytic activity of the catalysts.

The photoluminescence emission spectra are useful study to investigate the efficiency of charge carrier trapping, immigration, and transfer to understand the fate of electron–hole pairs in semiconductor photocatalysts [36,38]. Fig. 6 shows the photoluminscence spectra of TiO_2, Cu–TiO_2 and Cu–TiO_2/GR composites. It can be seen from the spectra that PL intensity of pure TiO_2 is much higher than those of Cu–TiO_2 and Cu–TiO_2/GR samples, indicating that Cu doping and graphene can efficiently inhibit the recombination of

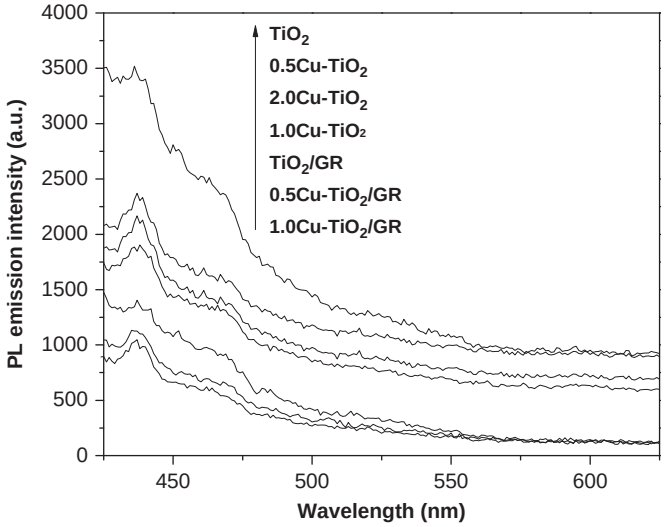

Fig. 6. Photoluminescence spectra of pure TiO_2, Cu–TiO_2 and 1.0Cu–TiO_2/GR composites with excitation wavelength of 380 nm.

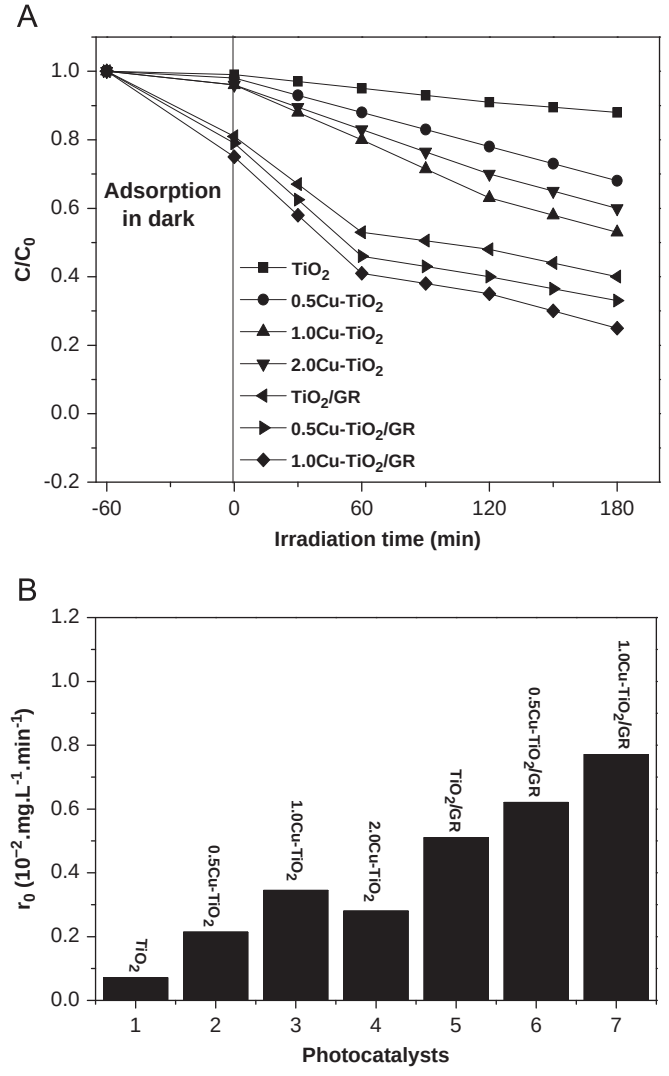

Fig. 7. (A) Photocatalytic degradation curves of Cu–TiO_2 and Cu–TiO_2/GR with various Cu contents as a function of time and (B) initial degradation rate of MO in the presence of various photocatalytsts.

photogenerated electrons and holes. Further inspection of PL spectra reveals that 1.0Cu–TiO_2/GR composite sample has the lowest PL intensity compared to other samples, which shows that optimal loading of Cu with graphene has reduced the recombination of excited electrons and holes.

The photocatlytic degradation of methyl orange with Cu–TiO_2 and Cu–TiO_2/GR composites catalysts under visible light is displayed in Fig. 7A. About 25% adsorption of MO was observed for 1Cu–TiO_2/GR composite catalyst after stirring for 1 h in dark, which is higher than those of all other samples and it increased to some extent in comparison to Cu–TiO_2 and TiO_2/GR composite. The initial degradation rate of MO with different photocatalysts follows roughly the pseudo-first-order reaction kinetics at low dye concentrations [24]:

$$\ln(C_0/C) = k_{app}\, t$$

where k_{app} is the apparent constant, and it was used as the basic kinetic parameter for different photocatalysts. C_0 is the initial concentration of MO in aqueous solution and C is the residual concentration of MO at time t. The apparent constant values could be deduced from the linear fitting of $\ln(C_0/C)$ versus irradiation time. The initial degradation rate ($r_0 = k_{app} \times C_0$) of 10 mg L^{-1} MO with different catalysts was studied and the results are presented in Fig. 7B.

Fig. 7A shows enhanced photocatalytic activity of copper doped TiO_2 nanoparticles with respect to that of pure TiO_2 under visible light irradiation. Photoactivity was increased gradually with increasing Cu–TiO_2 ratio up to 1.0%. Further increase of copper loading did not enhance the photocatalytic activity of the catalyst. This may be due to the fact that t he excess doping of copper ions into TiO_2 lattice introduced recombination centers, which are detrimental to the photocatalytic activity of the catalyst [11]. The degradation rate of MO (Fig. 7B) follows the order 1.0Cu–TiO_2/GR > 0.5Cu–TiO_2/GR > TiO_2/GR > 1.0Cu–TiO_2 > 2.0Cu–TiO_2 > 0.5Cu–TiO_2 > TiO_2. The degradation rate constant for the 1.0Cu–TiO_2/GR composite catalyst ($r_0 = 0.77 \times 10^{-2}$/min) was found to be ca. 11 times higher in comparison to pure TiO_2 ($r_0 = 0.07 \times 10^{-2}$/min). The possible reasons for enhanced photocatalytic activity of composite catalyst under visible light irradiation are the following. Firstly, the enhanced photocatalytic activity of Cu–TiO_2/GR composite catalyst might be attributed to extended light absorption into visible light region due to copper doping and graphene incorporation. Secondly, in Cu–TiO_2/GR system, the excited electrons of TiO_2 could transfer from the conduction band to graphene through percolation mechanism [23]. Thus, in the composite, graphene served as an acceptor of generated electrons of TiO_2 and effectively suppressed the charege recombination, leaving more charge carriers to form reactive species and promote the degradation of MO [23]. Thirdly, the higher adsorption of MO (25%) onto the catalyst surface also played a role in enhancing the photocatalytic activity of composite catalyst. For the simple reason when more organic molecules are adsorbed on the catalyst surface, there is a greater probability of reaction. The photoformed electrons that are produced

during photocatalysis can readily transfer to the doped copper through the graphene and then easily reduce dioxygen or other electron accepter groups present in the aqueous medium. As a result, electron–hole recombination is largely prevented and this further facilitates the production of more OH radicals due to the valence band of TiO_2 and the superoxide radicals anion (O_2^-) at the surface of catalyst, which in turn result in a faster degradation of organics [28].

4. Conclusion

Cu–TiO_2/GR composite photocatalysts were prepared by a hydrothermal method. It was found that all Cu–TiO_2/GR composite catalysts showed enhanced photocatalytic activity than pure TiO_2 under visible-light irradiation for MO degradation. The higher photocatalytic activity of the composite catalyst could be attributed to the synergistic effects of extended light absorption, efficient charge separation, enhaced adsorptivity on the composite catalyst surface due to two-dimensional planar structure of graphene and possibility of more π–π interaction between composite and organic compound.

Acknowledgments

This work was supported partially by the Natural Science Foundation of China (No. 51072180), China Postdoctoral Science Foundation (No. 20110491764), the Fundamental Research Funds for the Central Universities (No.2009QNA4005), and the State Key Laboratory of Silicon Materials (SKL2009-14) at Zhejiang University. N.R. Khalid thanks Higher Education Commission of Pakistan for IRSIP scholarship.

References

[1] X. Li, R. Xiong, G. Wei, Journal of Hazardous Materials 164 (2009) 587.
[2] S. Ardizzone, C.L. Bianchi, G. Cappelletti, S. Gialanella, C. Pirola, V. Ragaini, Journal of Physical Chemistry C 111 (2007) 13222.
[3] M. Li, P. Tang, Z. Hong, M. Wang, Colloids and Surfaces A:Physicochemical and Engineering Aspects 318 (2008) 285.
[4] M. Li, Z. Hong, Y. Fang, F. Huang, Materials Research Bulletin 43 (2008) 2179.
[5] R. Asahi, T. Morikawa, T. Ohwaki, K. Aoki, Y. Taga, Science 293 (2001) 269.
[6] J.M. Herrmann, Catalysis Today 53 (1999) 115.
[7] M. Li, S. Zhou, Y. Zhang, G. Chen, Z. Hong, Applied Surface Science 254 (2008) 3762.
[8] J. Wang, D.N. Tafen, J.P. Lewis, Z. Hong, A. Manivannan, M. Zhi, M. Li, N.Q. Wu, Journal of the American Chemical Society 131 (2009) 12290.
[9] D. Tafen, J. Wang, N.Q. Wu, J.P. Lewis, Applied Physics Letters 94 (2009) 093101.
[10] G. Colon, M. Maicu, M.C. Hidalgo, J.A. Navio, Applied Catalysis B: Environmental 67 (2006) 41.
[11] L.S. Yoong, F.K. Chong, B.K. Dutta, Energy 34 (2009) 1652.
[12] C. Chen, X. Li, W. Ma, J. Zhao, H. Hidaka, N. Serpone, Journal of Physical Chemistry B 106 (2002) 318.
[13] Z. Xiong, L.L. Zhang, X.S. Zhao, Journal of Chemistry European 17 (2011) 2428.
[14] H. Yu., H. Irie, K. Hashimoto, Journal of the American Chemical Society 132 (2010) 6898.
[15] T. Arai, M. Yanagida, Y. Konishi, A. Ikura, Y. Iwasaki, H. Sugihara, K. Sayama, Applied Catalysis B 84 (2008) 42.
[16] S. Fukahori, H. Ichiura, T. Kitaoka, H. Tnaka, Environmental Science and Technology 37 (2003) 1048.
[17] A.M. Turek, I.E. Wachs, E.De Canio, Journal of Physical Chemistry 96 (1992) 5000.
[18] J. Aguado, R. Van Grieken, M.J. Lopez-Munos, J. Marugan, Journal of Applied Catalysis A 312 (2006) 202.
[19] J. Matos, A. Garcia, P.S. Poon, Journal of Materials Science (2010) 1.
[20] J. Matos, A. Garcia, T. Cordero, J.M. Chovelon, C. Ferronato, Catalysis Letters 130 (2009) 568.
[21] K. Woan, G. Pyrigiotakis, W. Sigmund, Advanced Materials 21 (2009) 2233.
[22] D. Wang, D. Choi, J. Li, Z. Yang, Z. Nie, R. kou, D. Hu, C. Wang, L.V. Saraf, J. Zhang, ACS Nano 3 (2009) 907.
[23] H. Zhang, X. Lv, Y. Li, Y. Wang, J. Li, ACS Nano 4 (2009) 380.
[24] S. Wang, S. Zhou, Journal of Hazardous Materials 185 (2011) 77.
[25] X.Y. Zhang, H.P. Li, X.L. Cui, Y. Lin, Journal of Materials Chemistry 20 (2010) 2801.
[26] G. Williams, B. Seger, P.V. Kamat, ACS Nano 2 (2008) 1487.
[27] D.Choi Wang, D. Li, J. Yang, Z. Nie, Z. Kou, R. Hu, D. Wang, C. Saraf, L.V. Zhang, J. Aksay, I.A. Liu, ACS Nano 3 (2009) 907.
[28] B. Neppolian, A. Bruno, C.L. Bianchi, M. Ashokkumar, Ultrasonics Sonochemistry 19 (2012) 9.
[29] N. Farhangi, R.R. Chowdhury, Y. Medina-Gonzalez, M.B. Ray, P.A. Charpentier, Applied Catalysis B: Environmental (2011).
[30] Y. Su, Y. Xiao, Y. Li, Y. Du, Y. Zhang, Materials Chemistry and Physics 126 (2011) 761.
[31] W.S. Hummers, R.E. Offeman, Journal of the American Chemical Society 80 (1958) 1339.
[32] N.R. Khalid, Z. Hong, E. Ahmed, Y. Zhang, H. Chan, M. Ahmad, Applied Surface Science 258 (2012) 5827.
[33] K. Song, J. Zhou, J. Bao, Y. Feng, Journal of the American Chemical Society 91 (2008) 1369.
[34] J. Liu, H. Bai, Y. Wang, Z. Liu, X. Zhang, D.D. Sun, Advanced Functional Materials 20 (2010) 4175.
[35] B. Erdem, R.A. Hunsicker, G.W. Simmons, E.D. Sudol, V.L. Dimonie, M.S. El-Aasser, Langmuir 17 (2001) 2664.
[36] Y. Wu, J. Zhang, L. Xiao, F. Chen, Applied Surface Science 256 (2010) 4260.
[37] S.Y. Treschev, P.W. Chou, Y.H. Tseng, J.B. Wang, E.V. Perevedentseva, C.L. Cheng, Applied Catalysis B: Environmental 79 (2008) 8.
[38] K. Akihiko, N. Ryo, I. Akihide, K. Hideki, Chemical Physics 339 (2007) 104.